molecular pharmaceutics

articles

Oxidized Mesoporous Silicon Microparticles for Improved Oral Delivery of Poorly Soluble Drugs

Feng Wang,[†] He Hui,[‡] Timothy J. Barnes,[†] Christian Barnett,[§] and Clive A. Prestidge*,[†]

Ian Wark Research Institute, University of South Australia, Mawson Lakes, SA, 5095, Australia, Sansom Institute, University of South Australia, Adelaide, SA 5000, Australia, and pSiMedica Ltd, Malvern Hills Science Park, Geraldine Road, Malvern, WR14 3SZ, U.K.

Received September 2, 2009; Revised Manuscript Received October 26, 2009; Accepted October 29, 2009

Abstract: Surface functionalized mesoporous silicon (pSi) microparticles are reported as a solid dispersion carrier for improving dissolution and enhancing the orally administered pharmacokinetics (fasted rat model) of indomethacin (IMC), employed as a model poorly soluble BCS type II drug. IMC was loaded via immersion/solvent evaporation onto the thermally oxidized pSi particles, which provide a stable hydrophilic matrix with a nanoporous structure. The solid state properties of IMC loaded pSi were characterized by Fourier transform infrared spectroscopy, X-ray powder diffraction, differential scanning calorimetry and thermogravametric analysis. IMC molecules are encapsulated in a noncrystalline state due to geometric confinement in the nanopores; stability of the noncrystalline state has been demonstrated for several months under accelerated storage conditions. The pSi carrier facilitates accelerated immediate release of IMC and enhanced oral delivery performance in comparison with crystalline indomethacin and Indocid i.e. a 4-times reduction on T_{max}, a 200% increase on C_{max} and a significant increase in bioavailability. The *in vitro*−*in vivo* correlation is discussed based on the noncompartment model and gives insight into the delivery mechanism for the pSi carrier.

Keywords: Poorly soluble drugs; porous silicon; solid state stability; *in vitro* dissolution; *in vivo* pharmacokinetics; *in vitro*−*in vivo* correlation (IVVC)

Introduction

There is considerable interest in improving the oral delivery of poorly water-soluble active pharmaceutical ingredients (APIs), for example, they were recently found to comprise ∼30−40% of the top 200 oral drug products from the US, Britain, Spain and Japan.[1] Under the biopharmaceutics classification scheme (BCS)[2] poorly water-soluble APIs may be further classified as either high or low intestinal permeability (corresponding to BCS class II or IV, respectively). Therefore, for BCS class II APIs, improving the solubility can be used to facilitate a corresponding increase in bioavailability. Common approaches to improving API aqueous solubility include complexation,[3] use of cosolvents,[4] solid dispersions,[5−8] formulation of API nanoparticles[9] or lipid carriers,[10,11] or control of the API's polymorphic form.[12−17]

* Author to whom correspondence should be addressed. Mailing address: University of South Australia, Ian Wark Research Institute, Mawson Lakes Campus, Mawson Lakes, South Australia, 5095. Tel: +61 8 8302 3569. Fax: +61 8 8302 3683. E-mail: Clive.Prestidge@unisa.edu.au.

[†] Ian Wark Research Institute, University of South Australia.

[‡] Sansom Institute, University of South Australia.

[§] pSiMedica Ltd.

(1) Takagi, T.; Ramachandran, C.; Bermejo, M.; Yamashita, S.; Yu, L. X.; Amidon, G. L. A Provisional Biopharmaceutical Classification of the Top 200 Oral Drug Products in the United States, Great Britain, Spain, and Japan. *Mol. Pharmaceutics* **2006**, *3* (6), 631–643.

(2) Amidon, G. L.; Lennernäs, H.; Shah, V. P.; Crison, J. R. A Theoretical Basis for a Biopharmaceutic Drug Classification: The Correlation of in Vitro Drug Product Dissolution and in Vivo Bioavailability. *Pharm. Res.* **1995**, *12* (3), 413–420.

10.1021/mp900221e © **2010 American Chemical Society**
Published on Web 10/29/2009

Currently, the major challenges faced in the formulation of poorly soluble drug delivery systems are the solid state stability and the establishment of a reliable *in vitro*−*in vivo* (IVIV) correlation. Considerable attention has focused on the preparation of amorphous forms of poorly soluble APIs; however, this approach presents numerous formulation stability challenges since the high energy amorphous form tends to undergo molecular reordering to the more thermodynamically stable crystalline form.[18−20] Environmental factors play a critical role in determining the amorphous−crystalline transformation rate, in particular temperature and humidity, hence these must be controlled by either formulation excipients or packaging.[14] Similarly, the presence of residual "seed" crystalline material in an amorphous formulation may also accelerate the solid state recrystallization process.

Solid dispersions typically involve incorporation of the poorly soluble API with polymeric excipients, such as polyethylene glycol,[7] polyvinylpyrrolidone[8] or hydrogels.[21] More recently, however, several inorganic materials such as mesoporous silica,[22−24] clay particles[25] and lipid−inorganic hybrids[10,11] have been employed. These highly porous materials typically possess nanometer sized pores, providing both a large effective surface area and a hydrophilic surface. Due to spatial confinement within a nanosized pore, crystalline drug molecules are normally unable to form highly ordered crystals, instead remaining in noncrystalline or amorphous forms.

Mesoporous silicon (pSi) was initially developed for use in optoelectronic devices after the discovery of its unique photoluminescent properties;[26] however, more recently pSi has been considered for use in a range of applications

(3) Casella, R.; Williams, D. A.; Jambhekar, S. S. Solid-state [beta]-cyclodextrin complexes containing indomethacin, ammonia and water. II. Solubility studies. *Int. J. Pharm.* **1998**, *165* (1), 15–22.

(4) DiNunzio, J. C.; Miller, D. A.; Yang, W.; McGinity, J. W.; Williams, R. O., III. Amorphous Compositions Using Concentration Enhancing Polymers for Improved Bioavailability of Itraconazole. *Mol. Pharmaceutics* **2008**, *5* (6), 968–980.

(5) Fini, A.; Cavallari, C.; Ospitali, F. Raman and thermal analysis of indomethacin/PVP solid dispersion enteric microparticles. *Eur. J. Pharm. Biopharm.* **2008**, *70*, 409–420.

(6) Kennedy, M.; Hu, J.; Gao, P.; Li, L.; Ali-Reynolds, A.; Chal, B.; Gupta, V.; Ma, C.; Mahajan, N.; Akrami, A.; Surapaneni, S. Enhanced Bioavailability of a Poorly Soluble VR1 Antagonist Using an Amorphous Solid Dispersion Approach: A Case Study. *Mol. Pharmaceutics* **2008**, *5* (6), 981–993.

(7) Tran, P. H. L.; Tran, H. T. T.; Lee, B.-J. Modulation of microenvironmental pH and crystallinity of ionizable telmisartan using alkalizers in solid dispersions for controlled release. *J. Controlled Release* **2008**, *129* (1), 59–65.

(8) Lakshman, J. P.; Cao, Y.; Kowalski, J.; Serajuddin, A. T. M. Application of Melt Extrusion in the Development of a Physically and Chemically Stable High-Energy Amorphous Solid Dispersion of a Poorly Water-Soluble Drug. *Mol. Pharmaceutics* **2008**, *5* (6), 994–1002.

(9) Matteucci, M. E.; Brettmann, B. K.; Rogers, T. L.; Elder, E. J.; Williams, R. O., III; Johnston, K. P. Design of Potent Amorphous Drug Nanoparticles for Rapid Generation of Highly Supersaturated Media. *Mol. Pharmaceutics* **2007**, *4* (5), 782–793.

(10) Tan, A.; Simovic, S.; Davey, A. K.; Rades, T.; Prestidge, C. A. Silica-lipid hybrid (SLH) microcapsules: A novel oral delivery system for poorly soluble drugs. *J. Controlled Release* **2009**, *134* (1), 62–70.

(11) Simovic, S.; Heard, P.; Hui, H.; Song, Y.; Peddie, F.; Davey, A. K.; Lewis, A.; Rades, T.; Prestidge, C. A. Dry Hybrid Lipid-Silica Microcapsules Engineered from Submicron Lipid Droplets and Nanoparticles as a Novel Delivery System for Poorly Soluble Drugs. *Mol. Pharmaceutics* **2009**, *6* (3), 861–872.

(12) Crowley, K. J.; Zografi, G. Cryogenic grinding of indomethacin polymorphs and solvates: Assessment of amorphous phase formation and amorphous phase physical stability. *J. Pharm. Sci.* **2002**, *91* (2), 492–507.

(13) Schmidt, A. G.; Wartewig, S.; Picker, K. M. Potential of carrageenans to protect drugs from polymorphic transformation. *Eur. J. Pharm. Biopharm.* **2003**, *56* (1), 101–110.

(14) Strachan, C. J.; Rades, T.; Newnham, D. A.; Gordon, K. C.; Pepper, M.; Taday, P. F. Using terahertz pulsed spectroscopy to study crystallinity of pharmaceutical materials. *Chem. Phys. Lett.* **2004**, *390* (1−3), 20–24.

(15) Karjalainen, M.; Airaksinen, S.; Rantanen, J.; Aaltonen, J.; Yliruusi, J. Characterization of polymorphic solid-state changes using variable temperature X-ray powder diffraction. *J. Pharm. Biomed.* **2005**, *39* (1−2), 27–32.

(16) Masuda, K.; Tabata, S.; Kono, H.; Sakata, Y.; Hayase, T.; Yonemochi, E.; Terada, K. Solid-state 13C NMR study of indomethacin polymorphism. *Int. J. Pharm.* **2006**, *318* (1−2), 146–153.

(17) Muster, T. H.; Prestidge, C. Face specific surface properties of pharmaceutical crystals. *J. Pharm. Sci.* **2002**, *91* (6), 1432–1444.

(18) Newman, A.; Engers, D.; Bates, S.; Ivanisevic, I.; Kelly, R. C.; Zografi, G. Characterization of amorphous API:Polymer mixtures using X-ray powder diffraction. *J. Pharm. Sci.* **2008**, *97* (11), 4840–4856.

(19) Pan, X.; Julian, T.; Augsburger, L. Increasing the Dissolution Rate of a Low-Solubility Drug Through a Crystalline-Amorphous Transition: A Case Study with Indomethicin. *Drug Dev. Ind. Pharm.* **2008**, *34* (2), 221–231.

(20) Zhu, L.; Wong, L.; Yu, L. Surface-Enhanced Crystallization of Amorphous Nifedipine. *Mol. Pharmaceutics* **2008**, *5* (6), 921–926.

(21) Zahedi, P.; Lee, P. I. Solid molecular dispersions of poorly water-soluble drugs in poly(2-hydroxyethyl methacrylate) hydrogels. *Eur. J. Pharm. Biopharm.* **2007**, *65* (3), 320–328.

(22) Watanabe, T.; Hasegawa, S.; Wakiyama, N.; Kusai, A.; Senna, M. Comparison between polyvinylpyrrolidone and silica nanoparticles as carriers for indomethacin in a solid state dispersion. *Int. J. Pharm.* **2003**, *250* (1), 283–286.

(23) Chauhan, B.; Shimpi, S.; Paradkar, A. Preparation and evaluation of glibenclamide-polyglycolized glycerides solid dispersions with silicon dioxide by spray drying technique. *Eur. J. Pharm. Sci.* **2005**, *26* (2), 219–230.

(24) Takeuchi, H.; Nagira, S.; Tanimura, S.; Yamamoto, H.; Kawashima, Y. Tabletting of Solid Dispersion Particles Consisting of Indomethacin and Porous Silica Particles. *Chem. Pharm. Bull.* **2005**, *53* (5), 487–491.

(25) Aguzzi, C.; Cerezo, P.; Viseras, C.; Caramella, C. Use of clays as drug delivery systems: Possibilities and limitations. *Appl. Clay Sci.* **2007**, *36* (1−3), 22–36.

(26) Canham, L. T. Silicon quantum wire array fabrication by electrochemical and chemical dissolution of wafers. *Appl. Phys. Lett.* **1990**, *57* (10), 1046–1048.

including brachytherapy,[27] biosensing,[28,29] and both protein[30,31] and poorly soluble[32−34] API delivery. In contrast to conventional mesoporous silica, significant control of the pSi microstructure is possible. Typical pore dimensions range from 1 nm through to several micrometers, through control of the initial preparation conditions.[35] Another useful feature of pSi is its readily modified surface chemistry, using dry methods such as thermal oxidation[36,37] and thermal carbonization,[32] or wet methods including silane[29,38,39] and "click" chemistries.[40−42] The use of thermally carbonized pSi has been shown to reduce the release rate of model water-soluble APIs, whereas it was observed to enhance the release of poorly soluble APIs.[32] To date, however, we are unaware of any published *in vivo* studies for the delivery of either hydrophilic or poorly soluble drugs using pSi.

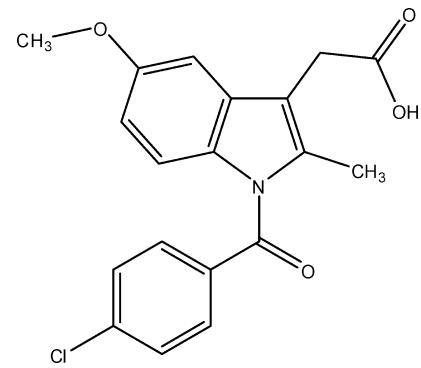

Figure 1. Molecular structure of indomethacin.

Indomethacin (IMC, Figure 1) is a nonsteroidal anti-inflammatory drug (NSAID) which is routinely used in the management of soft tissue inflammation often associated with trauma, osteoarthritis and rheumatoid arthritis.[43] IMC has two stable crystalline polymorphic forms, a poorly soluble γ-form (T_m = 161 °C) and a more water-soluble α-form (T_m = 155 °C). Amorphous IMC is typically prepared by melting the α-form (165 °C) followed by rapid quenching in liquid nitrogen.[44] Previously, it has been reported that mesoporous silica is able to stabilize amorphous IMC.[45,46]

In this study, we report on the development of a novel oral delivery system, using thermally oxidized pSi to stabilize the poorly soluble IMC in an amorphous solid dispersion. In particular, we aim to improve the orally dosed pharmacokinetics of IMC (e.g., bioavailability) compared to the commercially available Indocid formulation. The solid state properties of IMC-pSi-ox solid dispersions were characterized by Fourier transform infrared spectroscopy (FTIR), X-ray diffraction (XRD), differential scanning calorimetry (DSC), thermogravimetric analysis (TGA) and specific surface area analysis. Dissolution testing was used to evaluate

(27) Goh, A. S.-W.; Chung, A. Y.-F.; Lo, R. H.-G.; Lau, T.-N.; Yu, S. W.-K.; Cheng, M.; Satchithanantham, S.; Loong, S. L.-E.; Ng, D. C.-E.; Lim, B.-C.; Connor, S.; Chow, P. K.-H. A novel approach to brachytherapy in hepatocellular carcinoma using a phosphorous32 (32P) brachytherapy delivery device—a first-in-man study. *Int. J. Radiat. Oncol.* **2007**, *67* (3), 786–792.

(28) Pacholski, C.; Sartor, M.; Sailor, M. J.; Cunin, F.; Miskelly, G. M. Biosensing using porous silicon double-layer interferometers: Reflective interferometric Fourier transform spectroscopy. *J. Am. Chem. Soc.* **2005**, *127* (33), 11636–11645.

(29) Palestino, G.; Agarwal, V.; Aulombard, R.; Pérez, E.; Gergely, C. Biosensing and Protein Fluorescence Enhancement by Functionalized Porous Silicon Devices. *Langmuir* **2008**, *24* (23), 13765–13771.

(30) Prestidge, C. A.; Barnes, T. J.; Mierczynska-Vasilev, A.; Kempson, I.; Peddie, F.; Lau, C. H. Peptide and protein loading into porous silicon wafers. *Phys. Status Solidi A* **2008**, *205* (2), 311–315.

(31) Prestidge, C. A.; Barnes, T. J.; Mierczynska-Vasilev, A.; Skinner, W.; Peddie, F.; Barnett, C. Loading and release of a model protein from porous silicon powders. *Phys. Status Solidi A* **2007**, *204* (10), 3361–3366.

(32) Salonen, J.; Laitinen, L.; Kaukonen, A. M.; Tuura, J.; Bjorkqvist, M.; Heikkila, T.; Vaha-Heikkila, K.; Hirvonen, J.; Lehto, V. P. Mesoporous silicon microparticles for oral drug delivery: Loading and release of five model drugs. *J. Controlled Release* **2005**, *108* (2−3), 362–374.

(33) Salonen, J.; Kaukonen, A. M.; Hirvonen, J.; Lehto, V.-P. Mesoporous silicon in drug delivery applications. *J. Pharm. Sci.* **2007**, *97* (2), 632–653.

(34) Anglin, E. J.; Cheng, L.; Freeman, W. R.; Sailor, M. J. Porous silicon in drug delivery devices and materials. *Adv. Drug Delivery Rev.* **2008**, *60* (11), 1266–1277.

(35) Prestidge, C. A.; Barnes, T. J.; Lau, C.-H.; Barnett, C.; Loni, A.; Canham, L. Mesoporous silicon: A platform for delivery of therapeutics. *Expert Opin. Drug Delivery* **2007**, *4* (2), 101–110.

(36) Jarvis, K. L.; Barnes, T. J.; Badalyan, A.; Pendleton, P.; Prestidge, C. A. Impact of Thermal Oxidation on the Adsorptive Properties and Structure of Porous Silicon Particles. *J. Phys. Chem. C* **2008**, *112* (26), 9717–9722.

(37) Jarvis, K. L.; Barnes, T. J.; Prestidge, C. A. Aqueous and Thermal Oxidation of Porous Silicon Microparticles: Implications on Molecular Interactions. *Langmuir* **2008**, *24* (24), 1422–14226.

(38) Arroyo-Hernandez, M.; Martin-Palma, R. J.; Torres-Costa, V.; Duart, J. M. M. Porous silicon optical filters for biosensing applications. *J. Non-Cryst. Solids* **2006**, *352* (23−25), 2457–2460.

(39) Furbert, P.; Lu, C.; Winograd, N.; DeLouise, L. Label-Free Optical Detection of Peptide Synthesis on a Porous Silicon Scaffold/Sensor. *Langmuir* **2008**, *24* (6), 2908–2915.

(40) Ciampi, S.; Böcking, T.; Kilian, K. A.; James, M.; Harper, J. B.; Gooding, J. J. Functionalization of Acetylene-Terminated Monolayers on Si(100) Surfaces: A Click Chemistry Approach. *Langmuir* **2007**, *23*, 9320–9329.

(41) Britcher, L.; Barnes, T. J.; Griesser, H. J.; Prestidge, C. A. PEGylation of Porous Silicon Using Click Chemistry. *Langmuir* **2008**, *24* (15), 7625–7627.

(42) Ciampi, S.; Böcking, T.; Kilian, K. A.; Harper, J. B.; Gooding, J. J. Click Chemistry in Mesoporous Materials: Functionalization of Porous Silicon Rugate Filters. *Langmuir* **2008**, *24* (11), 5888–5892.

(43) Marion, W. F. V. Indomethacin in the treatment of soft tissue lesions: a double-blind study against placebo. *J. Int. Med. Res.* **1973**, *1*, 151–158.

(44) Andronis, V.; Zografi, G. Crystal nucleation and growth of indomethacin polymorphs from the amorphous state. *J. Non-Cryst. Solids* **2000**, *271* (3), 236–248.

(45) Takeuchi, H.; Nagira, S.; Yamamoto, H.; Kawashima, Y. Solid dispersion particles of amorphous indomethacin with fine porous silica particles by using spray-drying method. *Int. J. Pharm.* **2005**, *293* (1−2), 155–164.

(46) Watanabe, T.; Wakiyama, N.; Usui, F.; Ikeda, M.; Isobe, T.; Senna, M. Stability of amorphous indomethacin compounded with silica. *Int. J. Pharm.* **2001**, *226* (1−2), 81–91.

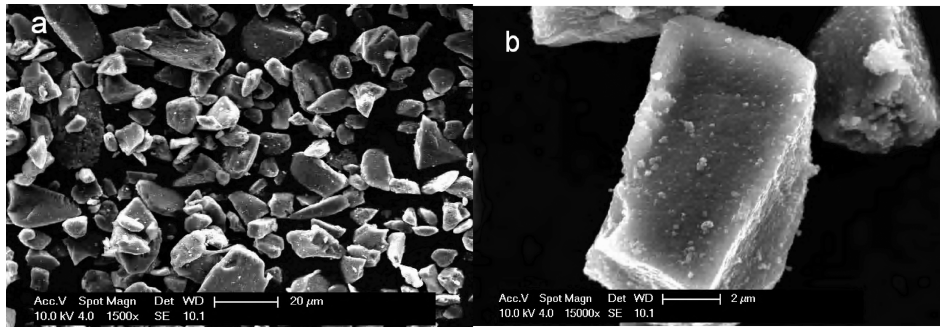

Figure 2. SEM images of IMC loaded pSi-ox: (a) full view and (b) a focus view.

Table 1. Summary of IMC-pSi-ox Sample Parameters, Including Average Size, Porosity, IMC Loading Level and Specific Surface Area, Pore Volume and Pore Size

sample	BET SSA (m^2/g)	pore vol (cm^3/g)	BJH_{des} pore size (nm)	IMC loading %
pSi-ox	321	0.542	8.8	n/a
IMC loaded pSi-ox	154	0.451	6.7	5.6

the *in vitro* performance of the IMC-pSi-ox formulation compared to powdered IMC and the Indocid formulation. The relative *in vivo* bioavailability of the three IMC formulations was assessed by oral dosing of Sprague−Dawley rats. Finally, we correlate the *in vitro* dissolution behavior with the *in vivo* bioavailability of each formulation.

Experimental Section

Materials. pSi microparticles were provided as gifts by pSiMedica Ltd. (U.K.). The preparation, in brief, was as follows: the p^+ silicon wafer was electrochemically anodized, and by controlling the parameters, the obtained pSi layer had the designated morphology, i.e. ~70% porosity, specific surface area (SSA) = 310.2 m^2/g and total pore volume (TPV) = 0.955 cm^3/g. The pSi layer was separated from the substrate and subsequently ground by jet milling. The pSi powder was further classified to particles with an average diameter of 13.6 μm ($d(0.1)$ = 7.8 μm and $d(0.9)$ = 23.1 μm, batch no. 8167R9BF, pSiMedica), as shown in Figure 2.

Indomethacin (purity >99.0%) was purchased from Sigma-Aldrich (Australia). Indocid capsules (25 mg dose of IMC, Merck Sharp & Dohme, batch no. J2556) were purchased from a local pharmacy. The contents of 10 capsules were mixed before an aliquot of this powder was investigated. All other chemicals were of analytical grade and used as received. High purity (resistivity >18.2 MΩ cm) water was used throughout the study.

Preparation of Indomethacin Loaded pSi-ox Microparticles. Thermally oxidized pSi was prepared by placing 500 mg of pSi particles in a ceramic crucible in a clean furnace at 600 °C in ambient atmosphere for 1 h; the sample is labeled as pSi-ox herein, and the physical properties are provided in Table 1. Amorphous IMC was prepared by melting the crystal IMC in a nickel crucible (165 °C) for 5 min, followed by quenching in liquid nitrogen.[44] The amorphous IMC glass was gently ground to a fine powder using a mortar and pestle.

A solvent partitioning/evaporation method was used to load IMC into pSi-ox particles. pSi powder (~500 mg) was transferred into 5 mL of IMC solution (chloroform, 10 mg/mL). After incubation for 6 h, the pSi particles were separated from the drug solution by filtration under vacuum. The wet pSi particles were stored in a fume hood cupboard for removal of solvent prior to oven drying at 60 °C for 1 h without additional chloroform rinsing. IMC loaded pSi particles are labeled as IMC-pSi-ox herein. The IMC content of the loaded pSi-ox particles was determined by a solvent extraction method, with 4 × 10 mL of ethanol used to extract IMC from 25 mg pSi particles. The pSi-ox particles were removed from solution by centrifugation (10,000 rpm), while the IMC content of the supernatant was determined by UV-spectroscopy (320 nm) from a previously determined standard calibration curve.

Physicochemical Characterization of IMC-pSi Microparticles. *Fourier-Transform Infrared Spectroscopy.* FTIR was carried out using a Nicolet Magna-IR 750 FTIR spectrometer (Nicolet Instrument Inc. USA) equipped with a liquid nitrogen cooled mercury−cadmium−telluride (MCT) detector and OMNIC software (version 4.1). KBr disks were prepared by weighing approximately 3 mg of free IMC or 10 mg of IMC-pSi-ox formulation for analysis, mixing with 300 mg of dried KBr in an agate mortar and pestle for approximately 2 min. Sample disks were prepared using a compression force of 10 tons using a 13 mm diameter round flat face punch for 4 min. Sample spectra were collected from 400 to 4000 cm^{-1} in transmission mode, with a resolution of 1 cm^{-1}. Each spectrum presented is the average of 128 scans.

Powder X-ray Diffraction (XRD). Powder XRD was carried out using a Philips model PW1050/25 goniometer, Philips model PW1130/90 X-ray high voltage power supply and Diffraction Technology gas proportional detector. The X-ray generator was operated at 45 kV and 35 mA using Co Kα (λ = 1.7902 Å) radiation. The diffracted beam was monochromated with a LiF crystal. The powder sample was scanned over the angular range of 10° (2θ) to 60° with a scan rate of 0.5°/min and step size of 0.02°.

Differential Scanning Calorimetry (DSC). DSC testing was performed using a modulated DSC 2920 (TA Instruments). Particle samples were accurately weighed to 5 ± 1 mg in

aluminum crimped pans. Testing was performed at temperatures increasing from 25 to 200 °C at a rate of 5 °C/min under nitrogen purging at a flow rate of 50 mL/min.

Thermal Gravimetric Analysis (TGA). A hi-res modulated TGA 2950 (TA Instruments) TGA was used to determine drug content. Approximately 10 mg of sample was placed in an open aluminum pan, and the temperature was increased from 25 to 550 °C, using a heating rate of 10 °C/min under nitrogen purging (50 mL/min).

Specific Surface Area Determination (N_2 Adsorption). Nitrogen adsorption isotherms were obtained at 77 K using a surface area and pore analyzer (Micromeritics, Gemini model 2380). Powder samples (~500 mg) were transferred to the sample bulb and evacuated to a pressure of 10^{-4} Pa at 80 °C overnight (>12 h) to remove physically adsorbed water prior to analysis. The Brumauer−Emmet−Teller specific surface area (BET-SSA) was estimated from the nitrogen adsorption data at the relative pressure (P/P^0) range from 0.06 to 0.20. The pore size distributions and pore volumes were calculated by the Barrett−Joiner−Halenda (BJH) method.

In Vitro Dissolution. In vitro dissolution was performed in 500 mL of phosphate buffer (0.05 M, pH 7.2) prepared according to USP30,[47] using a USP type II dissolution apparatus (paddle method) operating at 100 rpm. Each sample, containing ~15 mg of IMC, was predispersed in a small aliquot of dissolution medium prior to addition to the dissolution apparatus at 37.0 ± 0.5 °C. Aliquots of 5 mL were drawn at fixed time points and replaced with an equal volume of fresh dissolution medium. The sample aliquots were filtered through a 0.2 μm membrane (Acrodisc) to remove residual pSi microparticles prior to analysis.

***In Vivo* Absorption Study.** *Animal Experiments.* All animal experiments were approved by the Animal Ethics Committee, Institute of Medical and Veterinary Science (Adelaide, Australia). Groups of 4 male Sprague−Dawley rats weighing 330 ± 30 g were used for each absorption study. One group was dosed intravenously with 0.005 mmol of IMC in ethanol:propylene glycol:saline (2:2:6 v/v) solution. The remaining 3 groups were administered with a single dose (0.01 mmol IMC) by oral gavage using an aqueous suspension (0.7% w/v HPMC, 0.001% v/v acetic acid, pH 4.6) under light inhaled anesthesia; the 3 formulations considered include pure IMC, Indocid and IMC-pSi-ox.

The rats were cannulated in the right jugular vein under inhaled anesthesia and allowed to recover. The cannulated rats were fasted overnight (12 ± 1 h) prior to each oral dosing and were given access to food 4 h postdose, and water was accessible at all times. Blood samples (0.2 mL) were collected from the jugular vein at designated time intervals, and the cannula was flushed with an equal volume of heparinized normal saline (50 units/5 mL) to prevent blood clotting. The collected blood samples were centrifuged at 9400*g* for 10 min at 4 °C, and the collected plasma was stored at −20 °C prior to analysis. An aliquot of 100 μL of plasma was vortex-mixed with 100 μL of acetonitrile and centrifuged at 3500*g* for 10 min to remove proteins prior to HPLC analysis.

HPLC Assay for IMC. The IMC content in plasma was assayed using HPLC (Hewlett-Packard 1100) and consisted of a series of G1310A isopump, G1313 auto sampler, G1314A variable UV detector (Shimadzu Corporation, Japan) set at 320 nm, and a LiChrospher C_{18} analytical column (RP-18, 250 mm × 4.6 mm, 5 μm). The mobile phase was a mixture of methanol:acetonitrile:distilled water (60:20:20 v/v), containing 0.1% (v/v) glacial acetic acid, eluted at a flow rate of 1.0 mL/min and a sample injection volume of 20 μL. The limit of detection (LOD) and the limit of quantification (LOQ) of this analytical method were 40 ng/mL and 100 ng/mL, respectively. Prior to HPLC analysis, plasma aliquots of 100 μL were transferred to microcentrifuge tubes along with 10 μL of internal standard (acemetacin, 20 μg/mL) in mobile phase and 200 μL of acetonitrile containing 0.1% acetic acid. After vortex mixing for 1 min, the sample was centrifuged at 10000*g* for 10 min, and 200 μL of the supernatant was extracted for HPLC analysis. Linear calibration curves ($r^2 > 0.99$) were plotted for the ratio of acemetacin and IMC chromatographic peak areas against IMC concentration (in mobile phase solution) over the range 0.1 to 15 μg/mL. All analytes were diluted suitably to establish a final concentration in the range for HPLC quantification.

Pharmacokinetic Calculations. The pharmacokinetic parameters were obtained using the PC software, WinNonlin, Standard Edition Version 4.1 (Pharsight Corp.), using a noncompartmental model. The maximum plasma concentration (C_{max}) and the time at which it is reached (T_{max}) were determined directly from the individual plasma concentration−time profiles. The area under the concentration−time curve from $t = 0$ to infinity ($AUC_{0-\infty}$) was calculated using the linear trapezoidal rule. The values of $AUC_{0-\infty}$ obtained were used to estimate the absolute bioavailability (F) according to eq 1:

$$F = \frac{AUC_{0\rightarrow\infty}(\text{oral}) \times \text{dose(iv)}}{AUC_{0\rightarrow\infty}(\text{iv}) \times \text{dose(oral)}} \times 100\% \qquad (1)$$

Statistical Analysis. The pharmacokinetic data from the different formulations were analyzed statistically by one-way analysis variance (one-way ANOVA) with a least significant difference (LSD) posthoc test using SPSS 15.0 for Windows (SPSS Inc.). For all tests, the level of significance was set at $p \leq 0.05$.

Results and Discussion

Solid State Characterization of IMC-pSi-ox. The FTIR spectra obtained for the thermally oxidized pSi, crystalline and amorphous IMC and of IMC-pSi-ox are presented in Figure 3a, and the expanded wavenumber region 1200−1800 cm^{-1} is shown in Figure 3b. Characteristic features of the IMC FTIR spectra include peaks at 2900−3321 cm^{-1} (intermolecular OH) and 1716 and 1691 cm^{-1} (acid and

(47) USP30, *The United States Pharmacopeia 30 - National Formulary 25* ed.; US Pharmacopeia: 2007.

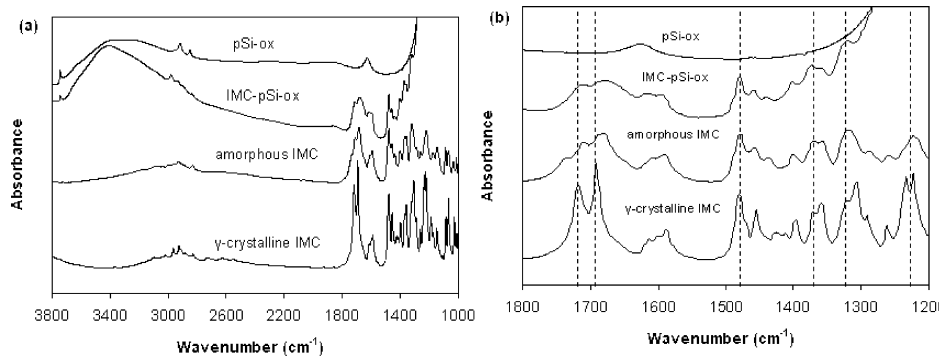

Figure 3. FTIR spectrum of pSi oxidized at 600 °C, IMC-pSi oxidized, amorphous and crystalline IMC, (a) full spectrum, 1000−3800 cm^{-1}, and (b) expanded spectrum, 1200−1800 cm^{-1}.

amide group carbonyl, respectively). Other peaks of note are found at 1397 cm^{-1} (−C−N− stretching), 1588, 1479 cm^{-1} (−C═C− stretching), 1453 cm^{-1} ($-CH_3$ bending), 1309 cm^{-1} (−C−O stretching, acidic group), 1230 and 1028 cm^{-1} (−C−O stretching, ether group), 1068 cm^{-1} (−C−Cl stretching) and 1269 cm^{-1} ($-CH_2-Cl$ bending), in agreement with spectra obtained for γ-crystalline IMC previously.[48,49] The amorphous IMC gives rise to a FTIR spectrum similar to that observed for the γ-crystalline IMC; however, the carbonyl stretch vibrations became broader and shifted to lower wavenumber, associated with dimer structure; while a shoulder presented at 1735 cm^{-1} which is assigned to the non hydrogen bonded carbonyl stretch of an end molecule of a chain.[48] The pSi-ox FTIR spectrum is relatively featureless, aside from the peaks at 3000−3500 cm^{-1} (Si−OH stretching) and at 1590 cm^{-1} (Si═O stretching). An absence of peaks in the region 2000−2400 cm^{-1} indicates that no residual $Si-H_x/O_y-SiH_x$ groups remain within the pSi mesoporous structure.[37]

In contrast, in the FTIR spectra of IMC loaded pSi-ox we observed a broad peak at 2800−3600 cm^{-1} (O−H stretching), while the originally strong carbonyl stretching peaks are weaker and broader and have shifted to lower wavenumbers of 1705 and 1674 cm^{-1}, and corresponding to the acid and amide groups, respectively, in agreement to the shift observed in FTIR spectrum of amorphous IMC. This suggests that the acid and amide functional groups are involved in hydrogen bonding with the pSi-ox surface.

DSC thermograms for pSi-ox, IMC-pSi-ox, amorphous and crystalline IMC are presented in Figure 4. A broad endotherm was observed for each of the pSi-ox containing samples below 100 °C, due to water loss from the hydrophilic pSi-ox. For the crystalline IMC, a single sharp exothermic melting peak at 161 °C was observed, in agreement with reported literature values for T_m of γ-crystalline IMC.[44] In contrast, amorphous IMC exhibited an exothermic peak at 108 °C associated with crystallization and a melting peak at

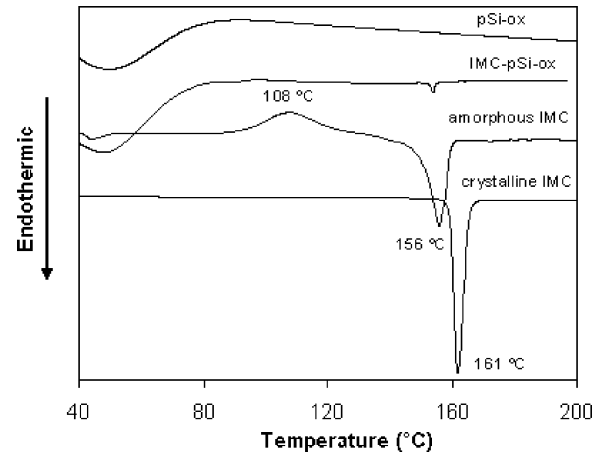

Figure 4. DSC scans of pSi ox, IMC-pSi ox, IMC-pSi ox physical mixture and the crystalline IMC.

156 °C that is consistent with T_m of metastable α-crystalline IMC form, respectively. This is attributed to a thermodynamic transition from amorphous to metastable crystalline IMC during the study.[50] For the IMC loaded pSi-ox, a small exothermic melting peak was observed at 155 °C, indicating the presence of a small amount of the metastable α-crystalline IMC form,[45] which is attributed to the presence of crystalline material on the surface of the pSi-ox particles or a thermodynamic transition from amorphous to metastable crystals during the study.[46] Further studies have shown no exothermic peaks across the temperature range considered, which suggests that the level of crystalline material is <5%.

TGA was performed on pSi-ox, crystalline IMC, the IMC loaded pSi-ox as well as an excess IMC/pSi-ox sample, with the derivative thermograms presented in Figure 5. We determined the IMC loading level in the pSi-ox samples to be ∼5.6%. For the pSi-ox sample, aside from water loss (<100 °C) we observed no change in weight over the entire temperature range considered (100−550 °C), whereas the crystalline IMC underwent thermal decomposition at ∼296 °C, with a single peak observed in the derivative thermogram. In contrast, for the IMC-loaded pSi-ox sample an IMC

(48) Taylor, L. S.; Zografi, G. Spectroscopic Characterization of Interactions Between PVP and Indomethacin in Amorphous Molecular Dispersions. *Pharm. Res.* **1997**, *14* (12), 1691–1698.

(49) Azarmi, S.; Ghaffari, F.; Lobenberg, R.; Nokhodchi, A. Mechanistic evaluation of the effect of thermal-treating on Eudragit RS matrices. *Farmaco* **2005**, *60* (11−12), 925–930.

(50) Bhugra, C.; Shmeis, R.; Pikal, M. J. Role of mechanical stress in crystallization and relaxation behavior of amorphous indomethacin. *J. Pharm. Sci.* **2008**, *97* (10), 4446–4458.

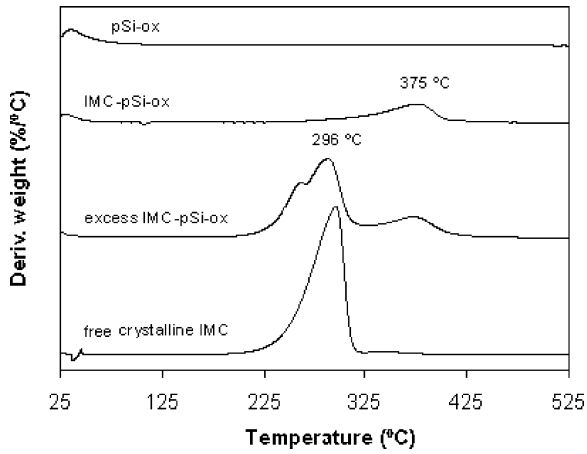

Figure 5. Derivative TGA thermograms of pSi-ox, IMC loaded pSi-ox, excess IMC loaded pSi-ox and crystalline IMC.

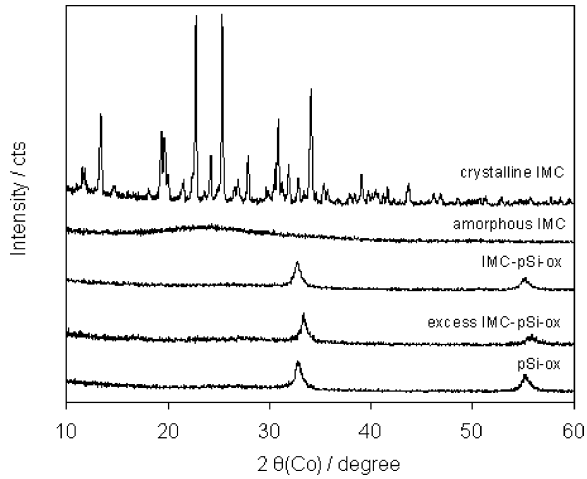

Figure 6. XRD diffraction patterns of crystalline and amorphous IMC, IMC loaded and excess IMC loaded pSi-ox and pSi-ox.

decomposition temperature of ~375 °C was observed, i.e. a significant increase from the 296 °C observed for the crystalline IMC.

For comparison, an excess loaded IMC-pSi-ox sample was prepared by drying the IMC-pSi solution rather than separating by filtration, to ensure the presence of IMC material external to the pSi pores. Two distinct decomposition steps/peaks are observed (Figure 5, curve b), corresponding to the bulk IMC as well as the encapsulated IMC. The slower decomposition of pSi-loaded IMC is attributed to restricted diffusion within the pSi nanoporous network.[51]

XRD diffraction patterns obtained for crystalline and amorphous IMC, IMC-pSi-ox and pSi-ox are presented in Figure 6. For crystalline IMC, we observed strong characteristic crystalline diffraction peaks (e.g., at $2\theta = 11.6°$, 13.4° and 19.4°) in good agreement with previously reported literature values for the γ-crystal form,[45,52] with small discrepancies attributed to differences in crystal size between samples.[53] As anticipated, the amorphous IMC did not exhibit any diffraction peaks. Two distinct diffraction peaks were observed for the pSi-ox, at 2θ values of 33° and 54°, which is in good agreement with the previous finding for oxidized pSi,[54] reflecting the crystalline features of pSi; while the broadness of the peaks was suggested as a result of X-ray diffuse scattering in the porous structure.[55] For both the IMC loaded pSi-ox and excess IMC-pSi-ox, we observed a diffraction pattern that was identical to that of the unloaded pSi-ox, indicating either an absence of any crystalline IMC material or that any crystalline material present is below the detection limit of the instrument. These observations suggest that the IMC is present within the pSi-ox matrix in an amorphous or molecular form.[45,56]

The specific surface area, pore volume and pore diameter of the IMC-pSi-ox samples from gas adsorption are presented in Table 1. Upon loading with IMC, we observed a decrease in specific surface area from ~230 to ~150 m^2/g for pSi-ox and IMC-pSi-ox, respectively, which corresponds to a 17% decrease (0.541 to 0.451 cm^3/g, respectively) in pore volume. This volume, however, is excess to the volume occupied by IMC molecules if calculation is based on IMC crystalline density of 1.37 g/cm^3,[44] suggesting some blockage of the nanoporous (<5 nm) structures might have occurred. The pSi-ox pore diameter calculated from the BJH desorption isotherm decreased from 8.8 to 6.7 μm upon IMC loading. This change in pore diameter is approximately equivalent to a monolayer of IMC molecules adsorbed on the inner surface of the pores, according to the IMC molecular size, *x*-, *y*- and *z*-axis, 8.5, 4.5, and 12.5 Å.[56]

To assess the solid state stability of the IMC-loaded pSi-ox formulation in comparison with amorphous IMC, samples were stored at 40 °C/75% relative humidity (RH). Individual samples were analyzed using both DSC and XRD at 1, 3, and 6 month time points, with the data presented in Table 2. The % crystallinity of each sample was determined from the melting endotherm of DSC thermograms, using

(51) Wu, C.; Bein, T. Conducting polyaniline filaments in a mesoporous channel host. *Science* **1994**, *264* (5166), 1757–1759.

(52) Otsuka, M.; Kato, F.; Matsuda, Y. Determination of indomethacin polymorphic contents by chemometric near-infrared spectroscopy and conventional powder X-ray diffractometry. *Analyst* **2001**, *126*, 1578–1582.

(53) Steele, G., Preformulation predictions from small amount of compound as an aid to candidate drug selection. In *Pharmaceutical preformulation and formulation—A practical guide from candidate drug selection to commercial dosage form*; Gibson, M., Ed.; CRC Press: New York, 2001; p 59.

(54) Ogata, Y. H.; Tsuboi, T.; Sakka, T.; Naito, S. Oxidation of Porous Silicon in Dry and Wet Environments under Mild Temperature Conditions. *J. Porous. Mater.* **2000**, *7* (1), 63–66.

(55) Bellet, D.; Dolino, G. X-ray diffraction studies of porous silicon. *Thin Solid Films* **1996**, *276* (1−2), 1–6.

(56) Kurozumi, M.; Nambu, N.; Nagai, T. Inclusion Compounds of Non-Steroidal Antiinflammatory and Other Slightly Water Soluble Drugs with α-and β-Cyclodextrins in Powdered Form. *Chem. Pharm. Bull.* **1975**, *23* (12), 3062–3068.

Table 2. Accelerated (40°C/75% RH) Solid State Stability of Standard (Amorphous) and pSi Loaded IMC

		stability time point (months)			
pSi-ox sample	assay	0	1	3	6
amorphous IMC	DSC (% crystallinity)	0.0	93.2	99.1	98.8
	XRD	A[a]	C[b]	C	C
pSi IMC	DSC (% crystallinity)	2.8	6.2	4.2	3.8
	XRD	A	A	A	A

[a] A: amorphous. [b] C: crystalline.

$$\%\ \text{crystallinity} = \frac{\Delta H_{\text{sample}}\ (\text{J/g})}{\Delta H_{\text{pureIMC}}\ (\text{J/g})} \qquad (2)$$

After 1 month, ~93% of the amorphous IMC sample had transformed to the more energetically stable crystalline form, with this value increasing to ~99% after 3 months of accelerated storage. In contrast, the IMC loaded pSi-ox exhibited a negligible change in crystallinity, after 6 months accelerated storage the % crystallinity increased from ~3% to ~4%.

XRD analysis confirmed the enhanced solid state stability under accelerated storage conditions, where, after 1 month, evidence of crystalline IMC was observed in the initially amorphous sample. In contrast, no evidence of crystalline IMC was observed in the XRD diffraction pattern obtained for the IMC loaded pSi-ox over 6 months.

In Vitro **Dissolution.** Dissolution profiles of crystalline IMC (γ-form), IMC-pSi-ox as well as the current marketed product, Indocid, are presented in Figure 7. Both IMC loaded pSi-ox and Indocid showed rapid dissolution, i.e. 85 and 95 wt % dissolved in the first 5 min, respectively. Complete (~100%) dissolution of the IMC was observed from the Indocid and pSi-ox formulations after ~10 and 30 min, respectively. Within the Indocid formulation, IMC is physically dispersed in a range of excipients, including lactose, lecithin, magnesium stearate, gelatin as well as colloidal silica.[57] As the IMC is present within the pSi-ox matrix as a molecular dispersion, i.e. the IMC is adsorbed to the pSi-ox surface, the necessary desorption process acts to limit the observed IMC release rate from the pSi matrix. In contrast, we observed a significantly reduced dissolution rate of the free crystalline IMC, with no dissolution plateau observed until ~80 min. This study highlights the role of both IMC crystalline form and formulation composition on the dissolution process.

In Vivo **Absorption Study.** IMC pharmacokinetics were determined for crystalline IMC powder, Indocid and IMC loaded pSi-ox using a fasted rat (Sprague−Dawley) model, dosed by oral gavage. Pure IMC was also dosed by iv for calculation of bioavailability. The mean plasma concentration versus time profiles for each IMC form is presented in Figure 8, and the pharmacokinetic parameters, calculated using a noncompartmental approach, are summarized in Table 3. For free IMC, values of C_{max} (2.5 ± 0.4 μg/mL), T_{max} (2.8 ± 0.7 h) and bioavailability (54 ± 3%) were obtained. Upon dosing with the Indocid formulation, we observed a significant increase in C_{max} (3.5 ± 0.5 μg/mL), a decrease in T_{max} (2.0 ± 0.0 h) and an increase in bioavailability (77 ± 4%). Delivery with the IMC-loaded pSi-ox formulation resulted in further significant increases in both C_{max} and bioavailability (6.5 ± 0.5 μg/mL and 100 ± 4%, respectively), along with a reduction in T_{max} (0.6 ± 0.3 h). These improvements in C_{max}, T_{max} and bioavailability were found to be statistically significant ($P < 0.03$).

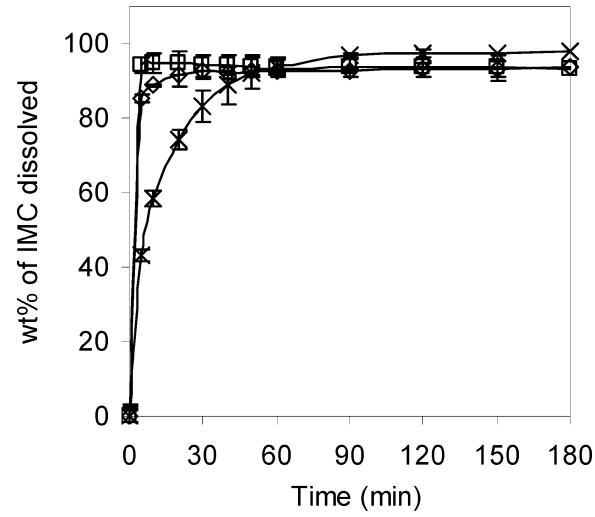

Figure 7. Dissolution profiles of IMC samples in phosphate buffer (pH 7.2): IMC loaded pSi-ox (◇), Indocid (□) and free crystalline IMC (×).

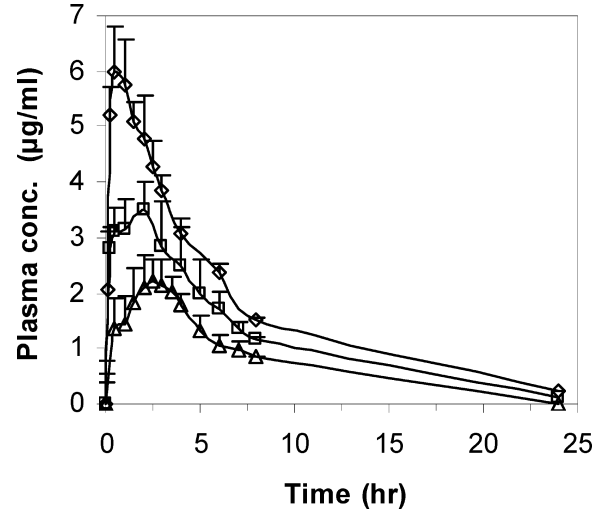

Figure 8. Plasma concentration profiles of IMC loaded pSi-ox (◇), Indocid (□) and free IMC (Δ) on fasted rat model by oral administration.

The main degradation product of pSi is orthosilicic acid ($Si(OH)_4$),[58] which is a normally excreted by the kidneys. The IMC-pSi-ox formulation was found to be well tolerated

(57) Merck&Co, Indocid(R): Consumer Medicine Information; Victorian Government, Australia: 1994; pp 1−3.

(58) Anderson, S. H. C.; Elliott, H.; Wallis, D. J.; Canham, L. T.; Powell, J. J. Dissolution of different forms of partially porous silicon wafers under simulated physiological conditions. *Phys. Status Solidi A* **2003**, *197* (2), 331–335.

Table 3. Pharmacokinetic Parameters for Free IMC (Iv and Oral Dosing), Oral Indocid and Oral pSi Formulations

	pure IMC			
pharmacokinetics parameter	iv	oral	Indocid (oral)	IMC-loaded pSi (oral)
dose (mmol)	0.005	0.01	0.01	0.01
T_{max} (h)	0	2.75 ± 0.65	2.00 ± 0.00	0.56 ± 0.31
C_{max} (μg/mL)		2.48 ± 0.38	3.49 ± 0.54	6.46 ± 0.52
AUC_{0-24h} (h·μg/mL/mg)	66.92 ± 6.73	35.83 ± 1.95	51.82 ± 2.33	66.98 ± 2.62
F (%)		53.54 ± 2.91	77.43. ± 3.9	100.1 ± 3.9

by the rats, with no adverse health effects observed during the study, in good agreement with previous studies demonstrating the lack of pSi cytotoxicity toward living cells.[59]

***In Vitro−in Vivo* Correlation (IVIVC).** Significant correlations between *in vitro* and *in vivo* data for IMC were investigated. Three levels of IVIVC are classified according to the US Food and Drug Administration.[60−62] Level A correlation is a point-to-point relationship between *in vitro* dissolution and *in vivo* absorption. Based on the data in Figure 8, the percentage of IMC absorbed at specific times was calculated from the plasma concentration data, as shown in Figure 9, using the method of Wagner and Nelson:[63,64]

$$\frac{A_T}{V_d} = C_T + K_{el}(\mathrm{AUC})_{t=0-T} \qquad (3)$$

where A_T is the amount of drug absorbed to time t, V_d is the apparent volume distribution, C_T is the blood concentration at time $t = T$, K_{el} is the elimination rate constant and the area under the curve between the limits $t = 0$ to $t = T$. A value of $K_{el} = 0.23\ h^{-1}$ was calculated from the slope obtained by a least-squares regression of the linear region of the log plasma concentration versus time profile for free IMC after intravenous dosing. Using this method, successive values of A_T/V_d are calculated to obtain the maximum $(A_T/V_d)_\infty$, which is then divided into each value of A_T/V_d to determine the percentage absorption data as a function of time.

Complete absorption (>90%) was observed for all 3 IMC formulations, however the time taken to reach maximum absorption increased from ~30 to 120 and 150 min for IMC-pSi-ox, Indocid and crystalline IMC, respectively. The absorption profiles for both the IMC-pSi-ox formulation and crystalline IMC are similar to their corresponding *in vitro* dissolution profiles, whereas Indocid exhibited significantly slower absorption compared to *in vitro* dissolution.

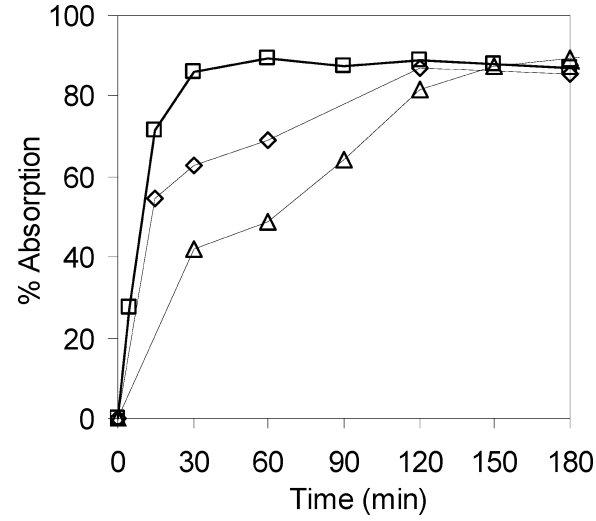

Figure 9. Absorption profiles of IMC loaded pSi-ox (□), Indocid (◇) and free IMC (Δ) generated from deconvolution of the corresponding plasma concentration profiles using the Wagner−Nelson method.

The Weibull model (eq 4) is an empirical equation routinely used to scale *in vitro* dissolution data for determining any IVIVC.[65]

$$\log\left[-\ln\left(1 - \frac{M_t}{M_\infty}\right)\right] = \beta \log(t + t_0) - \beta \log \alpha \qquad (4)$$

Fitting parameters (α, β) were used to calculate a time scale factor, which takes into account the intrinsic difference of time scales between *in vitro* release and *in vivo* absorption to enable direct comparison, by the following equation.[66]

(59) Coffer, J. L.; Whitehead, M. A.; Nagesha, D. K.; Mukherjee, P.; Akkaraju, G.; Totolici, M.; Saffie, R. S.; Canham, L. T. Porous silicon-based scaffolds for tissue engineering and other biomedical applications. *Phys. Status Solidi A* **2005**, *202* (8), 1451–1455.

(60) F.D.A. Guidance for Industry: Extended release Oral Dosage Forms: Development, Evaluation, and Application of In Vitro/In Vivo Correlations. 1997, p 27.

(61) Dressman, J. B.; Reppas, C. In vitro-in vivo correlations for lipophilic, poorly water-soluble drugs. *Eur. J. Pharm. Sci.* **2000**, *11* (Suppl. 2), S73–S80.

(62) Drewe, J.; Guitard, P. In vitro-in vivo correlation for modified-release formulations. *J. Pharm. Sci.* **1993**, *82* (2), 132–137.

(63) Sreenivasa Rao, B.; Seshasayana, A.; Pardha Saradhi, S. V.; Ravi Kumar, N.; Narayan, C. P. S.; Ramana Murthy, K. V. Correlation of 'in vitro' release and 'in vivo' absorption characteristics of rifampicin from ethylcellulose coated nonpareil beads. *Int. J. Pharm.* **2001**, *230* (1−2), 1–9.

(64) Wagner, J. G.; Nelson, E. Kinetic analysis of blood levels and urinary excretion in the absorptive phase after single doses of drug. *J. Pharm. Sci.* **1964**, *53* (11), 1392–1403.

(65) Li, S., Mueller-Zsigmondy; M. Yin, H., The role of in vitro-in vivo correlation in product development and life cycle management. In *Pharmaceutical Product Development: In vitro-In vivo Correlation*; Chilukuri, D. M., Sunkara, G.;,Young, D., Eds.; Informa: New York, 2007; Vol. 165, p 71.

(66) Brockmeier, D.; Voegele, D.; Von Hattingberg, H. M. In vitro-in vivo correlation, a time scaling problem? Basic techniques for testing equivalence. *Arzneim. Forsch.* **1983**, *33* (4), 598–601.

$$t_{invivo} = a + b \cdot t_{invitro} \quad (5)$$

where t_{invivo} = time in vivo, $t_{invitro}$ = time *in vitro*, a = lag time *in vivo* and b = time scale factor:[65]

$$b = \alpha_{invitro}/\alpha_{invivo}$$

For both the crystalline IMC and the IMC-pSi-ox formulation, we observed a linear relationship between *in vitro* dissolution and *in vivo* absorption, as shown in Figure 10, where

IMC-pSi-ox: % absorption=0.9857 × % dissolution (r^2 = 0.986)

crystalline IMC: % absorption = 0.9512 × %dissolution (r^2 = 0956)

The linear relationship observed for both IMC-pSi-ox and crystalline IMC samples indicate a level A IVIVC, i.e. *in vivo* absorption can be predicted from *in vitro* dissolution. As a class II drug, IMC has a high permeability; thus its rate of *in vivo* absorption is predicted to equal that of *in vivo* dissolution.[67] IMC has a pH dependent solubility (pK_a = 6.5), i.e. it is not soluble in gastric fluid, however it is soluble in the small intestine. For an immediate release formulation, the *in vitro* dissolution conditions should be relevant to the GIT environment,[68,69] hence, phosphate buffer (pH 7.2) was used as the dissolution medium, as recommended for IMC dissolution testing in the 30th USP.

It must be noted that that pSi-ox formulation has a value of $\alpha = 0.42$, which might be invalid, because it was obtained when 85 wt % of IMC has been released at the first time point (5 min), however, the precondition is that $\alpha = (T_d)^{\beta}$ where T_d is the time necessary to release 63.2 wt % of drug in the dosage form.[70] A time scale factor of 0.15 was calculated from the free IMC and was also used for the IMC-pSi-ox sample.[65]

It is hypothesized that the IMC-pSi-ox has a fast gastric transition time, due to the high specific gravity of pSi (silicon SG = 2.2) and the low pSi-ox solubility under acidic conditions, which suggests that the IMC-pSi-ox formulation rapidly delivers the IMC to the intestines, where it is dissolved and absorbed under the neutral conditions. This study represents the first reported use of pSi-ox to deliver a poorly soluble drug, where a level A IVIVC has been observed.

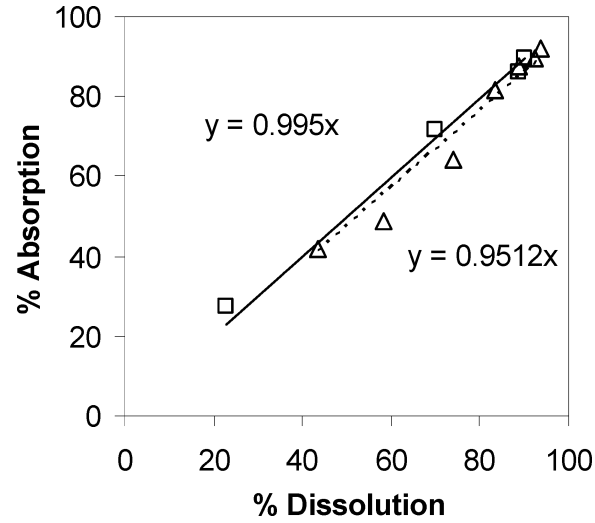

Figure 10. IVIVC of IMC loaded pSi-ox (□, solid trend line) and free IMC (Δ, dash trend line).

Conclusions

The successful development of an oxidized pSi based formulation for the delivery of poorly soluble drug indomethacin is reported. Indomethacin is present within the pSi-ox matrix in a noncrystalline form and the IMC-pSi-ox exhibits excellent 6-month solid state stability, under accelerated stability testing conditions (40 °C/75% relative humidity). Enhanced *in vivo* pharmacokinetics (increased C_{max} and bioavailability, decreased T_{max}) is demonstrated for the IMC pSi-ox formulation when compared with either pure IMC or a current commercially available formulation (Indocid). A level A correlation between *in vitro* dissolution and *in vivo* pharmacokinetic data has been established, in good agreement with the BCS (class 2) classification of indomethacin, i.e. poor solubility/high permeability. This work demonstrates the significant potential for the use of oxidized pSi as a novel delivery system for poorly soluble drugs.

Acknowledgment. The authors acknowledge the Australian Research Council Linkage grant scheme (LP0562379) and pSivida Ltd for funding. The authors gratefully acknowledge F. Peddie, Y. Song and Dr. A. Davey for useful discussions and thank Dr. Y. F. Xu, for assistance with the surface area/pore size measurement. F.W. acknowledges the Australian Research Council for his Australian Postgraduate Award (Industry) PhD scholarship.

MP900221E

(67) Löbenberg, R.; Amidon, G. L. Modern bioavailability, bioequivalence and biopharmaceutics classification system. New scientific approaches to international regulatory standards. *Eur. J. Pharm. Biopharm.* **2000**, *50* (1), 3–12.

(68) Galia, E.; Nicolaides, E.; Hörter, D.; Löbenberg, R.; Reppas, C.; Dressman, J. B. Evaluation of various dissolution media for predicting *in-vivo* performance of class I and II drugs. *Pharm. Res.* **1998**, *15* (5), 698–705.

(69) Nicolaides, E.; Galia, E.; Efthymiopoulos, C.; Dressman, J. B.; Reppas, C. Forecasting the *in-vivo* performance of four loow solubility drugs from their *in-vitro* dissolution data. *Pharm. Res.* **1999**, *16* (12), 1876–1882.

(70) Costa, P.; Lobo, S. M. J. Modeling and comparison of dissolution profiles. *Eur. J. Pharm. Sci.* **2001**, *13* (2), 123–133.